Energy & Environmental Science

RSC Publishing

PAPER

Charge transport in lithium peroxide: relevance for rechargeable metal–air batteries†

Cite this: *Energy Environ. Sci.*, 2013, **6**, 2370

Maxwell D. Radin[a] and Donald J. Siegel*[b]

The mechanisms and efficiency of charge transport in lithium peroxide (Li_2O_2) are key factors in understanding the performance of non-aqueous Li–air batteries. Towards revealing these mechanisms, here we use first-principles calculations to predict the concentrations and mobilities of charge carriers and intrinsic defects in Li_2O_2 as a function of cell voltage. Our calculations reveal that changes in the charge state of O_2 dimers controls the defect chemistry and conductivity of Li_2O_2. Negative lithium vacancies (missing Li^+) and small hole polarons are identified as the dominant charge carriers. The electronic conductivity associated with polaron hopping (5×10^{-20} S cm^{-1}) is comparable to the ionic conductivity arising from the migration of Li-ions (4×10^{-19} S cm^{-1}), suggesting that charge transport in Li_2O_2 occurs through a mixture of ionic and polaronic contributions. These data indicate that the bulk regions of crystalline Li_2O_2 are insulating, with appreciable charge transport occurring only at moderately high charging potentials that drive partial delithiation. The implications of limited charge transport on discharge and recharge mechanisms are discussed, and a two-stage charging process linking charge transport, discharge product morphology, and overpotentials is described. We conclude that achieving both high discharge capacities and efficient charging will depend upon access to alternative mechanisms that bypass bulk charge transport. More generally, we describe how the presence of a species that can change charge state – *e.g.*, O_2 dimers in alkaline metal-based peroxides – may impact rechargeability in metal–air batteries.

Received 12th May 2013
Accepted 24th June 2013

DOI: 10.1039/c3ee41632a

www.rsc.org/ees

Broader context

Li–air batteries are attracting increasing attention as a next generation energy storage technology thanks to their high theoretical energy densities. However, several challenges must to be addressed before these batteries can be viable. Two of these challenges, low rate capability and limited capacity, are believed to arise from sluggish charge transport within the discharge product, Li_2O_2. However, the mechanisms of transport in Li_2O_2 remain elusive. To shed light on this issue, we use first-principles calculations to predict the intrinsic electronic and ionic conductivity of Li_2O_2. We find that under discharge conditions crystalline Li_2O_2 is essentially insulating, while under moderate recharge overpotentials partial delithiation results in an appreciable conductivity. This unusual variation in conductivity with potential may explain why large Li_2O_2 particles can be decomposed at moderate overpotentials despite the otherwise insulating nature of this material. Perhaps more importantly, our results suggest a tradeoff between capacity and efficient recharging: achieving high capacities requires the formation of thick Li_2O_2 deposits, which will come at a cost of substantial overpotentials during charging. Consequently, alternative mechanisms that bypass bulk charge transport should be explored.

Introduction

Thanks to their high theoretical specific energy density, rechargeable non-aqueous Li–air batteries are attracting increasing attention as a future energy storage technology.[1–4] In the absence of undesirable side reactions (*e.g.* degradation of the electrolyte or carbon support[1,3,4]), a Li–air cell can be described by the reversible reaction $2Li + O_2 \leftrightarrow Li_2O_2$. This chemistry is unlike conventional Li-ion intercalation electrodes because the solid phase discharge product, lithium peroxide (Li_2O_2), nucleates and grows on the cathode during discharge, and subsequently decomposes during recharge.

In order to achieve a high energy density the cathode of a Li–air cell should be substantially filled with Li_2O_2 at the end of discharge. However, prior studies have suggested that charge transport limitations through an ostensibly insulating Li_2O_2 discharge phase may constrain the capacity and rate capability of Li–air cells.[5–9] Therefore, a question of both practical and fundamental importance to the Li–air system is the mechanism of charge transport through the discharge product.[10,11] For example, Viswanathan *et al.* have investigated electron tunneling through thin, dense films of Li_2O_2 and found that this

[a]*Department of Physics, University of Michigan, Ann Arbor, Michigan 48109, USA*
[b]*Department of Mechanical Engineering, University of Michigan, Ann Arbor, Michigan 48109, USA. E-mail: djsiege@umich.edu*

† Electronic supplementary information (ESI) available: Computational details, defect energetics, and a description of polaron hopping paths. See DOI: 10.1039/c3ee41632a

This journal is © The Royal Society of Chemistry 2013

mechanism cannot support appreciable currents beyond a thickness of ~5 nm.[5] Nevertheless, the high capacities measured in many experiments,[10,11] in conjunction with the observation of large discharge product particles (diameters up to ~1 micron or larger[10,11]) suggests that other charge transport mechanisms are at play.

Unfortunately, an accepted mechanism for charge transport in Li–air cathodes has yet to emerge.[5,12–19] First-principles calculations by Hummelshøj *et al.* predicted that a high concentration of lithium vacancies in Li_2O_2 will yield p-type conductivity associated with a depletion of electrons from the valence band.[12] Subsequent calculations have also predicted p-type conductivity at Li_2O_2 surfaces[17,18] and at Li_2O_2–carbon interfaces.[16] Other studies have predicted that both holes and electrons will become self-trapped in Li_2O_2, forming small hole[14] and small electron[15] polarons. Although hole polarons were at first predicted to have very low hopping barriers,[14] a recent study examining the mobilities of these species in more detail has challenged this notion.[19] Furthermore, the nature and concentrations of charge carriers and intrinsic point defects in Li_2O_2 have not been reported. Such information is important because the concentrations of these species, when combined with mobilities, relates to the conductivity of bulk Li_2O_2, and thus ties directly to the performance of the battery.

As a step towards elucidating the impact and mechanism of charge transport in Li–air cells, here we employ first-principles calculations to predict the conductivity of crystalline Li_2O_2. More specifically, the concentrations of all chemically-relevant intrinsic (point) defects in Li_2O_2 are evaluated as a function of cell voltage; subsequent calculations are used to assess the mobilities of the dominant charge carriers. To obtain an accurate description of the electronic structure, hybrid functionals[20,21] and many-body perturbation theory (*GW*) methods[22,23] are employed. Our calculations indicate that charge transport in Li_2O_2 is mediated by both the migration of negative lithium vacancies, V_{Li}^{-}, corresponding to missing Li^+, and the hopping of hole polarons, p^+. For ionic transport, the barrier for V_{Li}^{-} migration, 0.33–0.39 eV, yields an ionic conductivity of $\sim 4 \times 10^{-19}$ S cm^{-1}. The hopping of hole polarons was found to have in-plane and out-of-plane barriers of 0.42 and 0.71 eV, which are comparable to recent DFT+*U* calculations,[19] yet are much larger than those suggested by previous HSE06 calculations.[14] Consequently, we predict an intrinsic electronic conductivity of $\sim 5 \times 10^{-20}$ S cm^{-1}, which would classify Li_2O_2 as an insulator. During charging, the partial delithiation of Li_2O_2 is expected to increase the conductivity, with each overpotential increment of ~0.1 V increasing the conductivity by an order of magnitude. Such an enhancement may explain why Li–air cathodes that have been loaded with purchased Li_2O_2 can be recharged at high overpotentials despite the low conductivity of Li_2O_2.[24–27] Our results suggest that recharge may occur *via* a two-stage process, with thin deposits decomposing at low potentials *via* electron tunneling, and thick deposits decomposing at moderately high potentials *via* polaron hopping. Therefore, to minimize overpotentials, strategies for enhancing bulk transport – or avoiding altogether it in place of transport *via* other pathways such as surfaces, grain boundaries, amorphous regions, *etc.* – should be explored.

More generally, we discuss how the capability for electronic charge transport in metal–air discharge phases can be tied to the presence of a species that can change valence state, such as the O_2 dimers in Li_2O_2. The presence or absence of such a species could explain why some non-aqueous metal–air chemistries are rechargeable, while others are not.

Computational methodology

The crystal structure of Li_2O_2, shown in Fig. 1, consists of alternating layers of trigonal prisms and octahedra/tetrahedra, with oxygen sites lying on the vertices of the polyhedra. One notable feature of the structure is the presence of covalently bonded O_2 dimers. As we will describe later, the ability of these dimers to change charge state plays an important role in the defect chemistry and conductivity of Li_2O_2. All of the octahedra (O) and half of the trigonal prisms (TP) are occupied by lithium atoms.

Point defect formation energies were calculated for 23 unique species, including vacancies, divacancies, interstitials, polarons, and bipolarons. First principles calculations were performed using the Vienna *ab initio* simulation package (VASP)[28–31] with a $3 \times 3 \times 2$ (144-atom) supercell. Makov–Payne finite-size monopole corrections[32,33] and oxygen overbinding corrections[34–36] were included. See ESI† for details. All defect calculations were spin-polarized to account for open-shell configurations favored by some defects. Given that self-interaction errors inherent to semilocal functionals (*e.g.* GGAs) can lead to qualitatively incorrect descriptions of certain defects,[37–39] our calculations employ the HSE hybrid functional[20,21] in conjunction with many-body perturbation theory (*GW*) methods.[22,23] The incorporation of exact exchange in the HSE family of functionals serves to compensate for self-interaction error, with the mixing parameter α determining what fraction of the semilocal exchange is replaced with exact exchange. As is common practice, we have adjusted α to reproduce the bandgap from *GW*-based methods.[38–40] This approach is motivated by the fact that the positions of the band

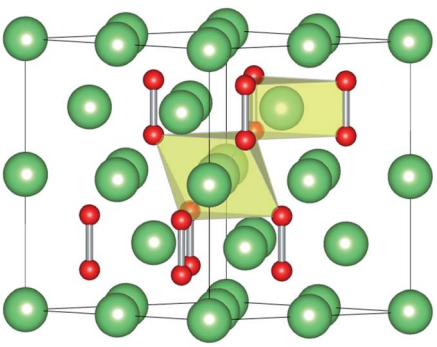

Fig. 1 Crystal structure of Li_2O_2, illustrated using a $2 \times 2 \times 1$ expansion of the unit cell. Large green atoms are lithium, and small red atoms are oxygen. Polyhedra indicate the trigonal prismatic and octahedral coordination of the two unique Li sites.

edges are important for determining defect properties. We find that a mixing parameter of $\alpha = 0.48$ yields a gap of 6.63 eV, which agrees well with the reference gap of 6.73 eV derived from an average of (non-self-consistent) G_0W_0 and self-consistent GW (scGW) calculations on bulk Li_2O_2 (see ESI† for details). As discussed below, we also investigated the sensitivity of our results to the choice of mixing parameter.

The equilibrium concentration C of a defect X in charge state q in a given solid phase can be written as $C(X^q) = D_X e^{-E_f(X^q)/k_B T}$, where D_X is the number density of defect sites.[41] Defect formation energies E_f are calculated according to:[33]

$$E_f(X^q) = E_0(X^q) - E_0(\text{bulk}) - \sum_i n_i\mu_i + q\varepsilon_F + E_{MP1}$$

where n_i is the number of atoms of the i^{th} species in the defect, μ_i is the chemical potential of that species, ε_F is the Fermi level, and E_{MP1} is the Makov–Payne monopole size correction.[32,33] Size convergence tests are reported in the ESI.† The chemical potential of oxygen was assumed to be fixed by equilibrium with oxygen in the atmosphere, while that of lithium was set by ion exchange with the anode:[12]

$$\mu_{Li}(\text{cathode}) = \mu_{Li}(\text{BCC Li}) - eE$$

where E is the cell voltage. Additional details are provided in the ESI.†

Results

Defect formation energies

Fig. 2 shows the formation energies for the low-energy defects as a function of the Fermi level for isolated Li_2O_2 (or equivalently, a cell whose potential is at the open circuit voltage). Table 1 summarizes the equilibrium formation energies and concentrations for all defects examined. As shown in Fig. 2, the dominant (*i.e.*, lowest energy) positively charged species is the hole polaron, p^+. The hole polaron consists of a hole that is self-trapped at an oxygen dimer, raising the formal charge on a peroxide (O_2^{2-}) dimer by one to yield a superoxide (O_2^{1-}) dimer and an associated contraction of the covalent O–O bond.[14,19] The dominant negative defect species is the negative lithium vacancy V_{Li^-} (*i.e.*, absence of a Li^+ ion). As shown in Table 1, negative lithium vacancies at the two symmetry-distinct Li sites have similar energies, with V_{Li}^- (TP) being only 20 meV more stable than V_{Li}^- (O). The concentrations of the dominant charge carriers, p^+ and V_{Li}^-, are established by an overall charge neutrality condition, and have values of 1×10^7 cm^{-3}, which is approximately three orders of magnitude less than the intrinsic carrier concentration in silicon at 300 K ($\sim 10^{10}$ cm^{-3}).[42] To quantify the influence of the mixing parameter, we also performed calculations using the "standard" α value of 0.25 (*i.e.* the HSE06 functional); this altered the equilibrium defect formation energies by only ~0.1 eV or less as shown in the ESI.† The influence of the mixing parameter is discussed in more detail below.

Table 1 Equilibrium defect formation energies (eV) and concentrations (cm^{-3}) in Li_2O_2

p^{2-}	3.12 (1×10^{-30})	$V_{O_2}^-$	2.47 (1×10^{-19})
p^-	1.51 (1×10^{-3})	$V_{O_2}^0$	4.71 (2×10^{-57})
p^+	0.95 (1×10^{7})	$V_{O_2}^+$	4.32 (1×10^{-50})
V_{Li}^- (O)	0.95 (3×10^{6})	$V_{O_2}^{2+}$	3.25 (9×10^{-33})
V_{Li}^- (TP)	0.93 (7×10^{6})	O_i^{2-}	4.55 (4×10^{-54})
V_{Li}^0 (O)	1.37 (4×10^{-1})	O_i^-	4.34 (1×10^{-50})
V_{Li}^0 (TP)	1.02 (2×10^{5})	O_i^0	1.33 (5×10^{0})
V_{Li}^+ (O)	2.05 (1×10^{-12})	O_i^+	2.22 (5×10^{-15})
V_{Li}^+ (TP)	1.45 (1×10^{-2})	Li_i^-	3.80 (1×10^{-41})
V_O^-	3.58 (4×10^{-38})	Li_i^0	2.51 (6×10^{-20})
V_O^0	0.74 (2×10^{10})	Li_i^+	1.69 (1×10^{-6})
V_O^+	1.66 (9×10^{-6})		

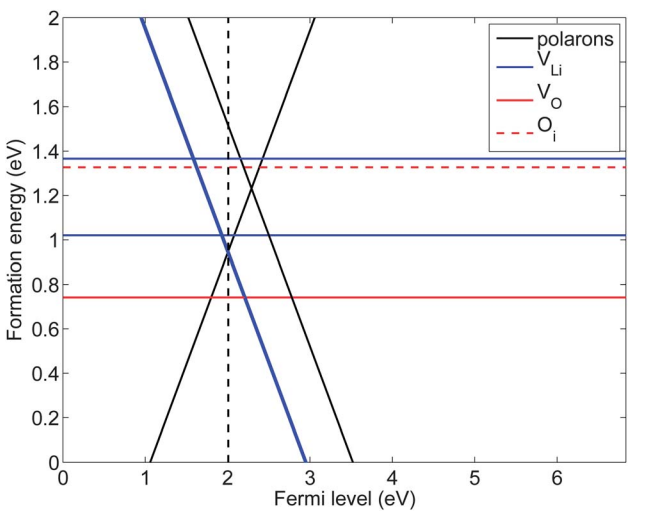

Fig. 2 Formation energies of low-energy defects in Li_2O_2. Positive defects have an upwards slope while negative defects have a downwards slope. The vertical dashed line indicates the position of the Fermi level that satisfies charge neutrality.

Fig. 2 also shows that the neutral oxygen vacancy is the most stable uncharged defect, with a formation energy of 0.74 eV. At first glance such a low formation energy may seem surprising because the creation of an oxygen vacancy requires the cleavage of an oxygen–oxygen bond. However, this cleavage results in the reduction of the remaining oxygen ion to a −2 charge state, which is energetically favorable. The second lowest energy neutral defect is the neutral lithium vacancy, V_{Li}^0 ($E_f = 1.02$ and 1.37 eV for the two Li sites), which consists of a p^+–V_{Li}^- bound pair. The binding energy $\Delta E = E_f(p^+) + E_f(V_{Li}^-) - E_f(V_{Li}^0)$ is 0.53 and 0.86 eV at the O and TP sites. A previous study[14] suggested that a hole polarons in Li_2O_2 would be bound to lithium vacancies on the basis that the p^+–V_{Li}^- binding is fairly strong. However, as can be seen from Table 1, the equilibrium concentrations of unbound p^+ and V_{Li}^- are in fact higher than that of V_{Li}^0 due to the entropy gain associated with dissociation.[41]

Defect mobilities

Conductivity in Li_2O_2 can in principle arise from the migration of charged defects (ionic conductivity) and/or hopping of small polarons (electronic conductivity). In both cases the

This journal is © The Royal Society of Chemistry 2013

conductivity depends on the concentrations and mobilities of these species, and can be expressed as:[43]

$$\sigma = \frac{Cva^2e^2}{k_B T} e^{E_b/k_B T},$$

where C is the concentration, ν is a hopping attempt rate that we take to be 10^{13} s^{-1},[15,44] a is the hop length, and E_b is the hopping barrier.

We first consider the ionic conductivity associated with V_{Li}^{-} migration. Energy barriers for five migration pathways were calculated using the nudged elastic band (NEB) method (see ESI†).[45] Because these calculations are computationally expensive, we optimized the migration pathway using the PBE GGA functional and report the barrier obtained at this level of theory;[46] this choice is justified by the fact that the unrelaxed barriers obtained with PBE were essentially the same as the unrelaxed barriers obtained with HSE, indicating that there is little sensitivity to the choice of functional. The lowest energy pathway corresponds to migration between adjacent octahedral and trigonal prismatic sites, with a barrier of 0.33 eV relative to the octahedral site and 0.39 eV relative to the trigonal prism site. Similar values have been found in prior calculations.[12,13] Setting E_b to the average of these two values yields an ionic conductivity of 9×10^{-19} S cm^{-1} and a defect diffusion coefficient of $D_i = \nu a^2 e^{E_b/k_B T} = 6 \times 10^{-9}$ cm^2 s^{-1}. Because this pathway allows for both in-plane and out-of-plane transport, the ionic conductivity is expected to be more or less isotropic.

Next we consider the electronic conductivity associated with hole polarons. In this case we evaluate the energy barrier associated with nearest neighbor hole polaron hopping. While previous studies treated all in-plane (*i.e.*, within a basal plane) hopping paths as symmetry equivalent and all out-of-plane paths as symmetry equivalent,[14,19] a Jahn–Teller distortion due to the degeneracy of π_x^* and π_y^* molecular orbitals breaks this symmetry. This distortion lowers the polaron's symmetry from D_{3h} to C_{2v} and lowers the ground state energy by 22 meV. As a result of this symmetry breaking there are six symmetry inequivalent in-plane and four symmetry inequivalent out-of-plane paths, as well as a trivial in-place rotation (see ESI†). We calculated the adiabatic barrier for these paths based on a chain of linearly interpolated images.[14,15] We found that all of the in-plane paths had similar barriers, and all of the out-of-plane paths had similar barriers (see ESI†). Attempts to optimize the geometry with the NEB method did not lead to significant changes in the barrier height: after 189 optimization steps, the barrier height of the lowest energy in-plane path was reduced by only 0.04 eV. Fig. 3 compares the energy profiles for the lowest energy in-plane and lowest energy out-of-plane hopping paths, for which we find barriers of 0.42 and 0.71 eV, respectively. These values correspond to conductivities of 5×10^{-20} and 1×10^{-24} S cm^{-1} for in-plane and out-of-plane transport, respectively. To place the calculated conductivities in context, we note that the conductivity of other battery materials can be orders of magnitude higher: for example, in $LiFePO_4$ $\sigma \sim 10^{-9}$ S cm^{-1},[47] while the conductivity of a good insulator such as fused silica is similar to our predicted value for Li_2O_2.[48]

Unlike lithium vacancy migration, hole polaron hopping is predicted to be anisotropic, with in-plane transport being favored over out-of-plane transport. It has previously been suggested that this anisotropy could contribute to anisotropies in the morphology of Li–air discharge products.[19] Combining the lithium vacancy defect diffusion coefficient D_i with the hole polaron defect diffusion coefficient ($D_p = 9 \times 10^{-10}$ and 2×10^{-14} cm^2 s^{-1} for in-plane and out-of-plane transport), we obtain a chemical diffusion coefficient[49] of $\tilde{D} = 2D_iD_p/(D_i + D_p) = 2 \times 10^{-9}$ and 4×10^{-14} cm^2 s^{-1} for in-plane and out-of-plane diffusion.

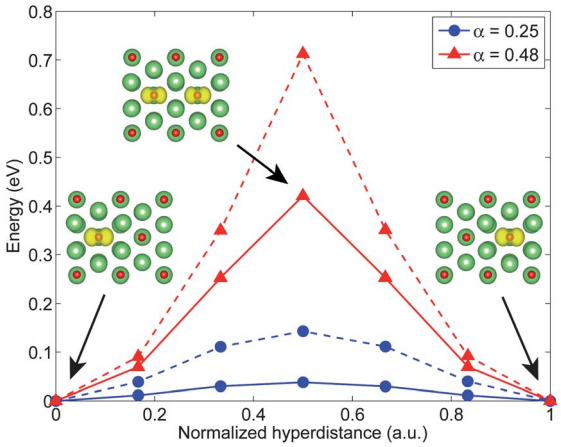

Fig. 3 Energy profiles for in-plane (solid lines) and out-of-plane (dashed lines) hole polaron hopping. Ball-and-stick models with magnetization density isosurfaces (yellow) are shown for in-plane hopping, as viewed along the *c* axis. Large green atoms are lithium, and small red atoms are oxygen.

Regarding experiments, a recent study measuring the ionic and electronic conductivities of Li_2O_2 arrived at qualitatively the same picture presented here: electronic conduction is mediated by hole polarons, and ionic conduction is mediated by negative lithium vacancies.[50] However, because the experimental sample was in the extrinsic regime – where defect concentrations are controlled by the presence of impurities – the measured electronic and ionic conductivities (at 100 °C) of 10^{-12} to 10^{-11} S cm^{-1} and 10^{-10} to 10^{-9} were significantly larger than those predicted here. Consequently, a direct comparison between experimental values and our calculations is not possible.

Another recent experimental study employed *in situ* TEM and found that the Li–O_2 discharge product decomposed at the Li_2O_2–carbon interface, but not the Li_2O_2–electrolyte interface, indicating that electronic charge transport is slower than Li ion transport.[51] This agrees with our calculations, which predict V_{Li}^{-} to be 18 times more mobile than hole polarons, based on the faster in-plane hopping rate. Furthermore, this study found that recharge of particles of radius $L \approx 200$ nm was visible at $t < 200$ s when a voltage of $V < 10$ V was applied across the particles. This indicates that V_{Li}^{-} can travel *at least* 200 nm in 200 s under a 10 V bias. This yields a lower bound on the mobility of lithium defects of $L^2/Vt = 2 \times 10^{-13}$ cm^2 V^{-1} s^{-1}. This is consistent with our calculations, which predict a higher V_{Li}^{-} mobility of $\mu = eD_i/k_B T = 2 \times 10^{-7}$ cm^2 V^{-1} s^{-1}. Discharge product composition, morphology, and temperature may introduce further complications in comparing our predictions to the experiment.

Finally, a third study has estimated the conductivity of the discharge product in Li–O_2 cells to be 10^{-12} to 10^{-13} S cm^{-1} based on electrochemical discharge–charge curves.[8] However, caution should be exercised in directly comparing these measurements to our calculations on crystalline Li_2O_2. First, the experiments were carried out at low capacities nominally resulting in Li_2O_2 deposits thin enough (<5 nm (ref. 8 and 5)) to support electron tunneling.[5] Second, it is well known that side reactions[1,3,4,52] can alter the composition (and presumably the conductivity) of the experimental discharge product, and also contribute to the observed current density.[53,54] Finally, morphological features in the experimental deposits (surfaces, grain boundaries, interfaces, amorphous regions, *etc.*)[16,17,55] may participate in transport, and these effects are not included in the present study.

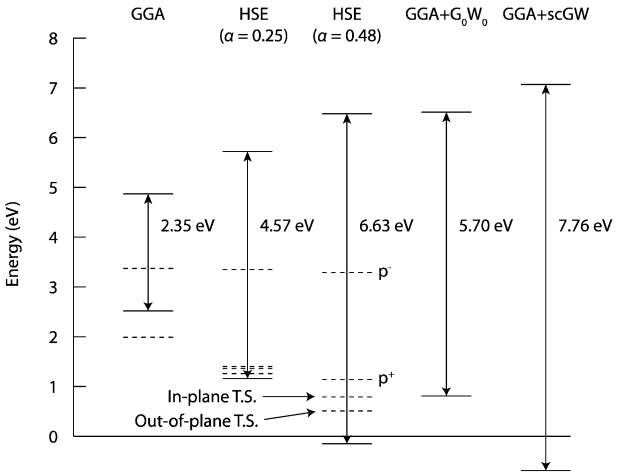

Fig. 4 Energy levels associated with the band edges, polaron ground states, and transition states for polaron hopping in Li_2O_2 as a function of calculation method. Energies are referenced to the average electrostatic potential, which is assigned a value of zero. All energies were calculated using the $\alpha = 0.25$ geometries, and finite size corrections were not included. Transition states are not shown for the PBE functional.

Influence of exchange-correlation functional

A recent DFT+U study ($U = 6$ eV) also reported hopping barriers comparable to the present values (0.39 to 0.48 eV), and noted that the barrier values were sensitive to the choice of U.[19] As the mixing parameter α in hybrid functionals is somewhat analogous to the U parameter in DFT+U, we likewise expect that the hopping barrier will also depend upon the choice of α. This is demonstrated in Fig. 3, which compares the energy profiles obtained with the two values of the mixing parameter explored: $\alpha = 0.25$ (*i.e.* the HSE06 functional[20,21]) and 0.48. The HSE06 calculation yields much smaller barriers of 38 and 143 meV, in good agreement with Ong *et al.*, who found barriers of 68 and 152 meV using the same functional.[14] To test geometry effects, we also calculated the $\alpha = 0.48$ barrier using the $\alpha = 0.25$ geometry. This lowered the in-plane and out-of-plane barriers by only 78 and 88 meV, indicating that the difference in barrier height between functionals is largely due to electronic structure effects.

As previously described, our predictions for the concentrations and hopping barriers for charge carriers in Li_2O_2 are based on an optimized choice for the fraction of exact change, α. Since other choices for α are possible, it is important to examine the influence of the mixing parameter upon polaron energy levels and their (hopping) transition states. Fig. 4 shows the energy levels (dashed lines) of the hole and electron polaron states, as determined from their formation energies referenced to the average electrostatic potential.[39,56] Three different values of α, corresponding to increasing amounts of exact exchange, are considered: 0, 0.25, and 0.48. [The $\alpha = 0$ case corresponds to the semilocal PBE GGA functional (*i.e.*, no exact exchange), $\alpha = 0.25$ corresponds to the HSE06 functional, and $\alpha = 0.48$ corresponds to the functional that reproduces the average Li_2O_2 bandgap predicted by G_0W_0 and self-consistent GW calculations (see prior discussion).] In systems where the atomic geometry and wavefunction do not change with α, the functional form of the HSE family[20,56] dictates that the energy will vary linearly with α. [Deviations from linearity indicate the degree to which the wavefunction (and geometry, if the atom coordinates are relaxed) is changing.] If the wavefunction and geometry are fixed, increasing amounts of exact exchange will increasingly penalize partially occupied orbitals;[57] that is, configurations with partially occupied orbitals should become higher in energy with increasing α. If the "correct" value of α is chosen, the penalty on partially occupied orbitals will exactly compensate for the self-interaction error from the semilocal exchange contribution.

The band edges for the three functionals, as well as those obtained with GW methods[22,23] are shown as solid lines in Fig. 4. Given that G_0W_0 and scGW band gaps typically bound the experimental band gap,[23,58] we expect that the positions of the G_0W_0 and scGW band edges likewise bound the positions of the experimental band edges. (Extra effort was taken to ensure convergence of the GW band edge positions, as these typically converge more slowly than the band gap;[39] see Fig. S2 in the ESI.†) Fig. 4 shows that the valence band edge falls while the conduction band edge rises as α increases. This is expected given that the valence and conduction states involve the partial depletion/filling of molecular orbitals.[57] Note that this variation is essentially linear in α, indicating that the valence and conduction band wavefunctions do not depend upon the choice of mixing parameter. The absolute value of the slope of this linear relation is somewhat larger for the valence band edge than the conduction band edge. The fact that the HSE06 valence band edge lies outside the range bounded by the GW edges suggests that a mixing parameter of $\alpha = 0.25$ is not sufficient to compensate the self-interaction error in Li_2O_2. On the other hand, a mixing parameter of $\alpha = 0.48$ places the valence band edge in better agreement with the GW calculations, indicating that this value gives a more realistic description of the electronic structure of Li_2O_2.

The data presented in Fig. 4 illustrates a fundamental difference regarding the stability of hole polarons in Li_2O_2 as described by the semi-local PBE ($\alpha = 0$) *vs.* hybrid functionals ($\alpha = 0.25$ and 0.48). In both hybrid functionals the position of

 This journal is © The Royal Society of Chemistry 2013

the valence band maximum (VBM) lies below the hole polaron level. In contrast, the hole polaron level lies above the VBM in PBE. Consequently, charge depletion in PBE generates delocalized holes in the top of the valence band, whereas localized holes (polarons) are predicted by the hybrid functionals. (In order to make an apples-to-apples comparison, the energy levels in Fig. 4 were determined using single-point energy calculations performed on the $\alpha = 0.25$ geometries. Releasing this constraint in PBE results in delocalization of the hole throughout the cell.) By comparing the PBE band edges to the *GW* band edges we can see that this instability is an artifact of self-interaction error.[38,39,57] This behavior is consistent with that of defects in other systems where semilocal functionals predict delocalized electrons, in contradiction to experimental measurements.[37,38]

Although PBE favors delocalized holes over hole polarons, Fig. 4 shows that the hole polaron is actually more stable in PBE than in the hybrid functionals when referenced to the average electrostatic potential. This is because as the mixing parameter is reduced the hole polaron begins to spread out and hybridize with the valence band, resulting in partial occupancies of the oxygen p states and consequently a ground state energy that is too negative; see Fig. S1 in the ESI.† Although the energy levels in Fig. 4 show that HSE06 ($\alpha = 0.25$) favors hole polarons over delocalized holes, the difference in energy between these two may be smaller than errors associated with finite-size effects and numerical convergence (see Fig. S6 in the ESI†); this raises some doubt as to the relative stability of delocalized holes and hole polarons in HSE06.[14]

As an aside, we note that the self-interaction errors inherent to GGAs are not limited to charged defects. Consider the neutral lithium vacancy, V_{Li}^0. The hybrid functionals predict this to consist of a V_{Li}^-–p^+ bound pair, whereas PBE instead delocalizes the hole over several nearby oxygen sites. The resulting partial occupancy of oxygen p states and concomitant self-interaction error causes PBE to overbind this defect by as much as 1 eV relative to the hybrid functionals (see ESI†). Indeed, a prior study using a GGA functional found a formation energy for V_{Li}^0 of 2.85 eV (referenced to bulk metallic Li), while a subsequent study using HSE06 found higher formation energies of 3.8 and 4.1 eV (TP and O sites, respectively). Our $\alpha = 0.48$ calculations yield similar values when referenced to metallic Li (3.98 and 4.33 eV).

Regarding the energy barriers for polaron hopping, we note that these transition states exhibit partial occupancy because the polaron is split between two different sites. Consequently, the energy levels of the transition states are sensitive to the choice of mixing parameter. Fig. 4 illustrates the energy levels of the transition states for the in-plane and out-of-plane hopping pathways given in Fig. 3. This analysis also explains the variation of the hopping barrier with the choice of *U*, which also penalizes partially occupied orbitals.[19] As discussed above, the HSE06 mixing parameter of 0.25 is not large enough to compensate for self-interaction errors in Li_2O_2. The agreement with the DFT+*U* hopping barrier[19] (over the optimal range of *U* values based on experimental data) lends additional support to our choice of mixing parameter, $\alpha = 0.48$. Furthermore, our preliminary calculations based on Marcus theory[59] yield a similar value for the in-plane barrier.

Discussion

It is important to consider how the predicted conductivity could impact the performance of a Li–O_2 cell. To this end, we compare against performance targets for Li–air cells suggested in the literature.[60] We assume parameters based on the hypothetical bipolar plate-type Li–air battery described by Karulkar and Adams,[60] with the additional assumption that the discharge product grows as a uniform film on a porous cathode with a specific surface area of 100 $m^2\ g^{-1}$. Based on these assumptions, the discharge product should have a conductivity of $\sim 2 \times 10^{-11}$ S cm^{-1} in order to achieve an *iR* drop of less than 0.1 V (see ESI†). This target value is several orders of magnitude larger than the predicted intrinsic electronic conductivity (5×10^{-20} S cm^{-1}), suggesting that charge transport through bulk (crystalline) Li_2O_2 can be a performance-limiting factor. We note that the migration of negative lithium vacancies cannot sustain charge transport over long time periods because the cathode materials used in Li–O_2 cells (typically porous carbon) are effectively ion blocking.[61] For this reason we focus on the electronic conductivity provided by hole polaron hopping.

Discharge

As the predicted conductivity of Li_2O_2 is much smaller than that of other battery materials[47] it is tempting to conclude that charge transport through bulk Li_2O_2 is too small to play a meaningful role in a real cell. However, the conductivity is in principle not a fixed quantity, but can vary during discharge and charge because the cell potential impacts defect concentrations through variations in the lithium chemical potential. Fig. 5 shows the predicted electronic conductivity as a function of cell voltage *E*. The conductivity increases exponentially with *E* because higher potentials favor delithiation (*i.e.* the creation of negative lithium vacancies, which are charge compensated by

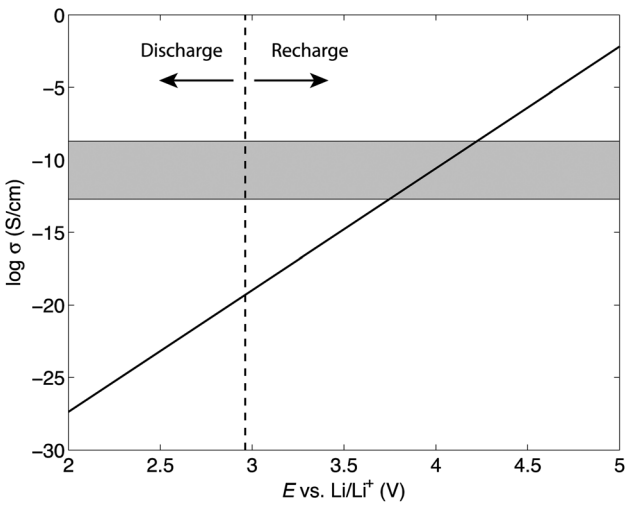

Fig. 5 Predicted electronic conductivity as a function of cell voltage. The dashed line indicates the open circuit voltage. The gray shaded region indicates the target conductivity needed to meet performance requirements, as discussed in the text.

hole polarons). Under discharge conditions ($E < E_{OCV}$) the bulk electronic conductivity is far below the target value, and therefore unable to supply significant charge transport. The fact that fairly high capacities and discharge product sizes are obtained in experiments[10,11] suggests two possibilities: (i) morphological features may locally enhance the conductivity of the discharge product; (ii) the oxygen reduction reaction (ORR) is not occurring at the Li_2O_2 surface, but rather at the carbon support or catalyst.

Fig. 6 summarizes the possible discharge mechanisms graphically. Fig. 6a–c show mechanisms in which the ORR occurs at the Li_2O_2 surface and would therefore require charge transport through the discharge product. Electron tunneling (Fig. 6a) cannot provide appreciable currents beyond a deposit thickness of ~5 nm,[5] and so this mechanism can occur only during the growth of thin deposits. Likewise, intrinsic conductivity (Fig. 6b) is predicted to be quite low under discharge conditions, as discussed above. Therefore neither tunneling nor bulk conduction can account for the observed growth of large discharge product particles.[10,11] If charge transport does occur through Li_2O_2 during discharge, we expect that it must be along extended defects such as surfaces,[17] interfaces,[16] grain boundaries, dislocations, or amorphous regions[55] that can enhance conductivity (Fig. 6c).

Fig. 6d and e illustrate mechanisms in which the ORR occurs not at the Li_2O_2 surface but rather at the surface of the carbon electrode (or catalyst). Fig. 6d shows a scenario in which reduction happens at an exposed region of the carbon/catalyst, followed by diffusion through the electrolyte or along surfaces of existing Li_2O_2. In this case the deposition of the discharge product is not an electrochemical step, but a chemical step.[10,55] Fig. 6e illustrates a more exotic scenario in which the ORR occurs at the buried carbon/Li_2O_2 interface; in this case, the reactants presumably diffuse through Li_2O_2 grain boundaries or other extended defects. Further investigation will be needed to explore these possibilities.

Recharge

Turning our attention to recharge, Fig. 5 demonstrates that recharge conditions are more conducive to charge transport compared to discharge. That is, for each 119 mV of charging overpotential the conductivity increases by one order of magnitude, such that a 0.5 V recharge overpotential would enhance the conductivity by 2×10^4, and a 1 V overpotential would enhance it by a factor of 3×10^8, bringing the intrinsic electronic conductivity close to the targeted values (grey region in Fig. 5). This effect results from an increase in the concentration of p^+ and V_{Li}^- charge carriers at higher potentials. These results suggest that hole polaron hopping may be rapid enough to account for the observed rechargeability of bulk Li_2O_2 particles at moderately high potentials.

Our prediction that fairly large overpotentials are needed to activate charge transport is in qualitative agreement with the high (3.5 to 4.2 V), yet relatively flat potential profiles obtained upon the charging of cathodes packed with purchased Li_2O_2 powders.[24–27] On the other hand, much lower potentials have been observed upon the initial charging of cells with thin films of Li_2O_2;[9] in this case charge transport can proceed *via* electron tunneling.[9,5] Thus these two morphologies apparently have very different recharge profiles. (We note that impurities in the reference Li_2O_2 samples could also influence charging behavior.[25])

Recent experiments have demonstrated that Li–O_2 cells can concurrently form both thin *and* thick deposits.[55,62] By combining the electron tunneling narrative with our prediction of enhanced polaronic conductivity at higher potentials we arrive at the following two-stage process linking charge

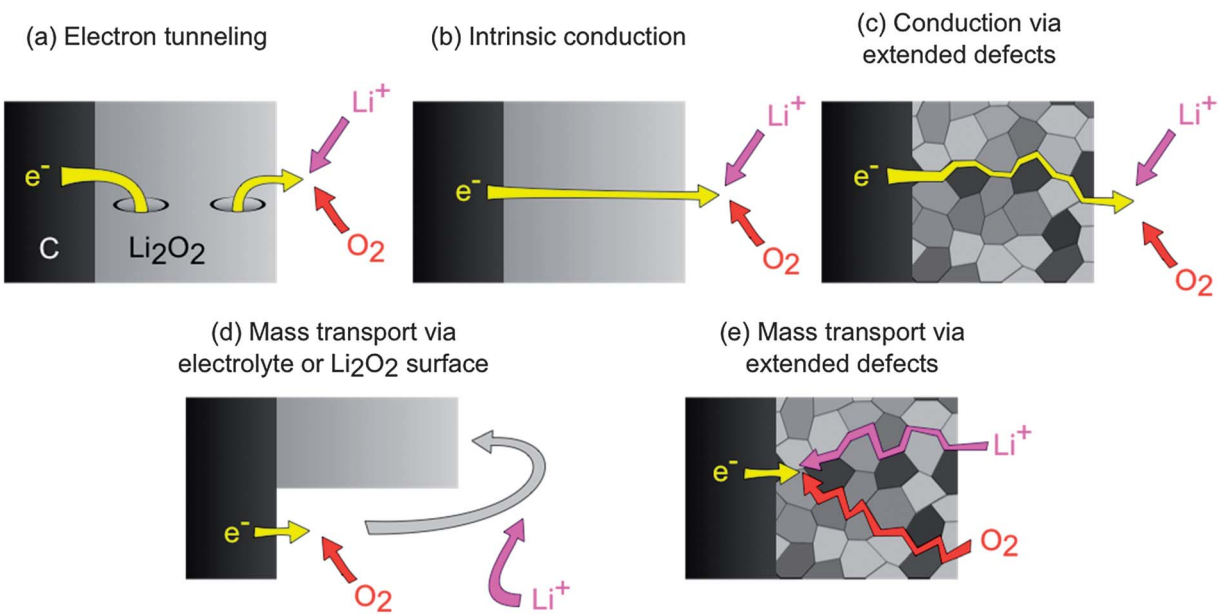

Fig. 6 Possible discharge mechanisms for a Li–air cell.

This journal is © The Royal Society of Chemistry 2013

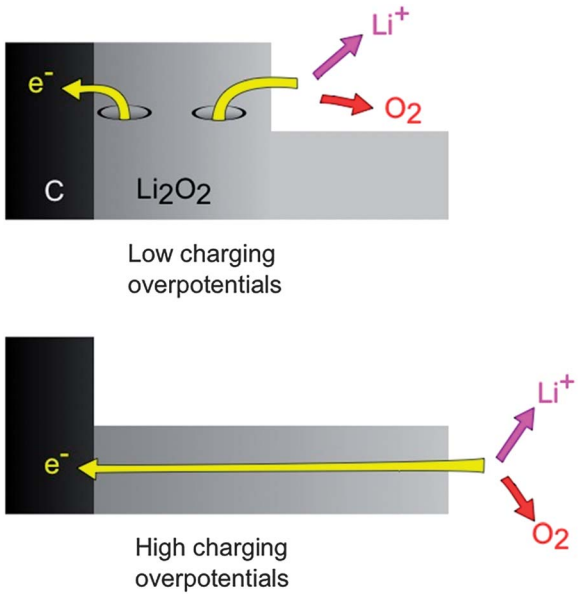

Fig. 7 Proposed two-stage recharge mechanism for a Li–air cell.

transport, particle morphology, and overpotentials during recharge, Fig. 7. Charging will initiate at low potentials due to the dissolution of thin Li_2O_2 deposits or decomposition at/near the Li_2O_2/electrolyte/carbon three-phase boundary. Charging will then conclude at high potentials where thick deposits decompose *via* polaron hopping. Side reactions involving the electrolyte or carbon support may of course introduce further complications.[1,3,4]

In support of the above mechanism, we note that experiments involving electrolyte/cathode combinations that minimize side reactions (such as DMSO + $LiClO_4$/nanoporous gold[5] or CH_3CN + $LiBF_4$/P50 (ref. 54)) yield charging profiles that start at low overpotentials and then rise to a plateau at overpotentials of roughly 1 V. Additionally, a recent study demonstrated a potassium air cell that discharged to potassium superoxide (KO_2), which is known to have a quite high room-temperature conductivity.[63] The low charging overpotentials observed in this experiment are consistent with the notion that sluggish charge transport in Li_2O_2 contributes to the recharge overpotentials in Li–O_2 cells.

If correct, our proposed mechanism implies that charge transport limitations will require moderately high overpotentials to recharge thick Li_2O_2 particles, *even if side reactions can be avoided*. Since high capacities likely require the formation of thick deposits, a tradeoff appears to exist between achieving both high capacities and efficient charging. Consequently, the ability to maximize capacity while simultaneously minimizing charging overpotentials will likely require accessing alternative reaction mechanisms that bypass bulk charge transport. Examples of such mechanisms would appear as the reverse of the processes shown in Fig. 6c–e.

We conclude by describing how the present results relate to other non-aqueous metal–air battery chemistries. More specifically, we speculate that the capability for even a modest amount of electronic charge transport in the discharge phase could explain why some non-aqueous metal–air chemistries are rechargeable at moderate potentials, while others are not. For example, Li_2O_2,[64–67] Na_2O_2,[68] NaO_2,[69] and KO_2 (ref. 70) can be electrochemically decomposed in non-aqueous environments; on the other hand Li_2O and SiO_2 are apparently electrochemically inactive in this context.[67,71–73] To rationalize these differences we recall that ionic solids in which the valence state can change tend to exhibit electronic conductivity due to the presence of charge carriers.[43,61] Examples include transition metal oxides in which the cation species can change its valence state (*e.g.*, TiO_2 or ZnO[43,61]). This differs, of course, from the behavior in peroxides and superoxides where it is the anion that can change valence state. The results presented here suggest that the presence of O_2 dimers in Li_2O_2, Na_2O_2, NaO_2, and KO_2 may contribute to the rechargeability of these materials in non-aqueous metal–air batteries by providing a pathway for charge transport through the bulk. Although in Li_2O_2 overpotentials are needed to activate charge transport, in other compounds such overpotentials may not be required to achieve sufficient conductivity. For example, (as previously mentioned) potassium superoxide is known to exhibit a high room temperature conductivity.[63]

Lending further support to this hypothesis, recent Raman and magnetic measurements have provided evidence of superoxide ions in the Li_2O_2 discharge product[74] as well as in synthesized Li_2O_2.[50] The presence of these ions confirms that O_2 dimers in Li_2O_2 can change their charge state between −2 and −1. In addition, prior calculations on surfaces[17,18] and on Li_2O_2 clusters[75] have identified superoxide-like dimers, and some alkali and alkaline earth metals are known to form mixed valence compounds in which peroxide and superoxide ions coexist.[76] In contrast, the absence of a species that can change valence state in Li_2O and SiO_2 may account for the electrochemical inertness of these materials. For example, prior simulations and experiments have found that intrinsic conduction in Li_2O is mediated by cationic Frenkel defects (*i.e.* Li_i^+ and V_{Li}^-),[77,78] and we do not expect the ionic conductivity associated with these defects to contribute to significant charge transport during cell operation because, as discussed above, the electrodes are ion-blocking.

Conclusions

In summary, we have performed a detailed analysis of charge transport mechanisms in the primary discharge product of non-aqueous Li–air batteries, Li_2O_2. We observe that the defect chemistry of Li_2O_2 is driven by the ability of O_2 dimers to change valence state, and our calculations predict that a cation deficiency in Li_2O_2 is charge-compensated by small hole polarons. The intrinsic electronic and ionic conductivities of Li_2O_2 are predicted to be comparable ($\sim 10^{-19}$ S cm^{-1}); the low bulk conductivity is therefore expected to limit the performance of Li–air cells. An enhancement of conductivity at high potentials where delithiation occurs may explain why bulk Li_2O_2 can nevertheless be decomposed electrochemically. Regarding computational methods, we find that the inclusion of exact exchange is essential for achieving a correct description of hole

polarons, and that care must be exercised in the choice of mixing parameter as this can have a large impact on the polaron hopping barrier.

We propose that recharge in Li–O_2 cells may occur by a two-stage process, with thin deposits decomposing at low potentials and thick deposits decomposing at high potentials. Such a mechanism implies that it will be challenging to achieve both high capacities and high round-trip efficiency simultaneously: attaining high capacities requires the formation of large/thick Li_2O_2 deposits, and we argue that decomposing these deposits requires substantial overpotentials during charging. Consequently, techniques for accessing alternative mechanisms that bypass bulk charge transport should be explored.

The presence of a species that can change its charge state may provide an important pathway for charge transport, and we propose that this feature explains why compounds containing O_2 dimers can be electrochemically decomposed in non-aqueous metal–air cells. This has implications for the development of other non-aqueous metal–air chemistries: for cations that cannot change charge state (*e.g.*, Li, Na, K, Mg), only peroxide and superoxide discharge products (and not oxides) would be expected to be rechargeable. On the other hand, transition metals that can change valence state in principle may yield rechargeable non-aqueous metal–air chemistries even if the discharge product is an oxide.

Acknowledgements

This work was supported by Robert Bosch LLC through the Bosch Energy Research Network Grant no. 19.04.US11 and the U.S. Department Energy's U.S.-China Clean Energy Research Center for Clean Vehicles, grant no. DE-PI0000012. P. Albertus, B. Kozinsky, G. Samsonidze, and C. Monroe provided helpful comments on a preliminary version of this manuscript.

Notes and references

1 J. Christensen, P. Albertus, R. S. Sánchez-Carrera, T. Lohmann, B. Kozinsky, R. Liedtke, J. Ahmed and A. Kojic, *J. Electrochem. Soc.*, 2012, **159**, R1.
2 G. Girishkumar, B. McCloskey, A. C. Luntz, S. Swanson and W. Wilcke, *J. Phys. Chem. Lett.*, 2010, **1**, 2193–2203.
3 D. Capsoni, M. Bini, S. Ferrari, E. Quartarone and P. Mustarelli, *J. Power Sources*, 2012, **220**, 253–263.
4 L. J. Hardwick and P. G. Bruce, *Curr. Opin. Solid State Mater. Sci.*, 2012, **16**, 178–185.
5 V. Viswanathan, K. S. Thygesen, J. S. Hummelshøj, J. K. Nørskov, G. Girishkumar, B. D. McCloskey and a. C. Luntz, *J. Chem. Phys.*, 2011, **135**, 214704.
6 P. Albertus, G. Girishkumar, B. McCloskey, R. S. Sánchez-Carrera, B. Kozinsky, J. Christensen and A. C. Luntz, *J. Electrochem. Soc.*, 2011, **158**, A343.
7 S. K. Das, S. Xu, A.-H. Emwas, Y. Y. Lu, S. Srivastava and L. a. Archer, *Energy Environ. Sci.*, 2012, **5**, 8927.
8 Y.-C. Lu and Y. Shao-Horn, *J. Phys. Chem. Lett.*, 2013, **4**, 93–99.
9 V. Viswanathan, J. K. Nørskov, A. Speidel, R. Scheffler, S. Gowda and A. C. Luntz, *J. Phys. Chem. Lett.*, 2013, **4**, 556–560.
10 Y.-C. Lu, B. M. Gallant, D. G. Kwabi, J. R. Harding, R. R. Mitchell, M. S. Whittingham and Y. Shao-Horn, *Energy Environ. Sci.*, 2013, **6**, 750.
11 A. Kraytsberg and Y. Ein-Eli, *Nano Energy*, 2012, DOI: 10.1016/j.nanoen.2012.11.016.
12 J. S. Hummelshøj, J. Blomqvist, S. Datta, T. Vegge, J. Rossmeisl, K. S. Thygesen, A. C. Luntz, K. W. Jacobsen and J. K. Nørskov, *J. Chem. Phys.*, 2010, **132**, 071101.
13 J. Chen, J. S. Hummelshøj, K. S. Thygesen, J. S. G. Myrdal, J. K. Nørskov and T. Vegge, *Catal. Today*, 2011, **165**, 2–9.
14 S. P. Ong, Y. Mo and G. Ceder, *Phys. Rev. B: Condens. Matter Mater. Phys.*, 2012, **85**, 081105.
15 J. Kang, Y. S. Jung, S.-H. Wei and A. Dillon, *Phys. Rev. B: Condens. Matter Mater. Phys.*, 2012, **85**, 035210.
16 Y. Zhao, C. Ban, J. Kang, S. Santhanagopalan, G.-H. Kim, S.-H. Wei and A. C. Dillon, *Appl. Phys. Lett.*, 2012, **101**, 023903.
17 M. D. Radin, J. F. Rodriguez, F. Tian and D. J. Siegel, *J. Am. Chem. Soc.*, 2012, **134**, 1093–1103.
18 M. D. Radin, F. Tian and D. J. Siegel, *J. Mater. Sci.*, 2012, **47**, 7564–7570.
19 J. M. García-Lastra, J. S. G. Myrdal, R. Christensen, K. S. Thygesen and T. Vegge, *J. Phys. Chem. C*, 2013, **117**, 5568–5577.
20 J. Heyd, G. E. Scuseria and M. Ernzerhof, *J. Chem. Phys.*, 2003, **118**, 8207.
21 A. V. Krukau, O. a. Vydrov, A. F. Izmaylov and G. E. Scuseria, *J. Chem. Phys.*, 2006, **125**, 224106.
22 M. Shishkin and G. Kresse, *Phys. Rev. B: Condens. Matter Mater. Phys.*, 2006, **74**, 035101.
23 M. Shishkin, M. Marsman and G. Kresse, *Phys. Rev. Lett.*, 2007, **99**, 246403.
24 W. Xu, V. V. Viswanathan, D. Wang, S. a. Towne, J. Xiao, Z. Nie, D. Hu and J.-G. Zhang, *J. Power Sources*, 2011, **196**, 3894–3899.
25 J. R. Harding, Y. Lu and Y. Shao-horn, *Phys. Chem. Chem. Phys.*, 2012, **14**, 10540–10546.
26 M. Song, D. Zhu, L. Zhang, X. Wang, L. Huang, Q. Shi, R. Mi, H. Liu, J. Mei, L. W. M. Lau and Y. Chen, *J. Solid State Electrochem.*, 2013, **17**, 2061–2069.
27 V. Anandan, R. Kudla, A. Drews, J. Adams and M. Karulkar, *ECS Trans.*, 2012, **41**, 167–174.
28 G. Kresse and J. Hafner, *Phys. Rev. B: Condens. Matter Mater. Phys.*, 1994, **49**, 14251–14269.
29 G. Kresse and J. Furthmüller, *Phys. Rev. B: Condens. Matter Mater. Phys.*, 1996, **54**, 11169–11186.
30 G. Kresse and J. Furthmüller, *Comput. Mater. Sci.*, 1996, **6**, 15–50.
31 G. Kresse and J. Hafner, *Phys. Rev. B: Condens. Matter Mater. Phys.*, 1993, **47**, 558–561.
32 M. C. Payne and G. Makov, *Phys. Rev. B: Condens. Matter Mater. Phys.*, 1995, **51**, 4014–4022.
33 H.-P. Komsa, T. Rantala and A. Pasquarello, *Phys. Rev. B: Condens. Matter Mater. Phys.*, 2012, **86**, 045112.

 This journal is © The Royal Society of Chemistry 2013

34 L. Wang, T. Maxisch and G. Ceder, *Phys. Rev. B: Condens. Matter Mater. Phys.*, 2006, **73**, 195107.
35 S. Kurth, J. P. Perdew and P. Blaha, *Int. J. Quantum Chem.*, 1999, **75**, 889.
36 J. S. Hummelshøj, A. C. Luntz and J. K. Nørskov, *J. Chem. Phys.*, 2013, **138**, 034703.
37 G. Pacchioni, *J. Chem. Phys.*, 2008, **128**, 182505.
38 W. R. L. Lambrecht, *Phys. Status Solidi B*, 2011, **248**, 1547–1558.
39 A. Alkauskas, P. Broqvist and A. Pasquarello, *Phys. Status Solidi B*, 2011, **248**, 775–789.
40 M. Choi, A. Janotti and C. G. Van de Walle, *J. Appl. Phys.*, 2013, **113**, 044501.
41 C. G. Van de Walle, *J. Appl. Phys.*, 2004, **95**, 3851.
42 a. B. Sproul and M. a. Green, *J. Appl. Phys.*, 1991, **70**, 846.
43 R. J. D. Tilley, *Defects in Solids*, John Wiley & Sons, Inc., 2008.
44 D. S. Sholl and J. A. Steckel, *Density Functional Theory: A Practical Introduction*, Wiley, Hoboken, NJ, 2009.
45 H. Jónsson, G. Mills and K. W. Jacobsen, Classical And Quantum Dynamics, in *Condensed Phase Simulations*, ed. B. J. Berne, G. Ciccotti and D. F. Coker, World Scientific, 1998, pp. 385–404.
46 J. P. Perdew, K. Burke and M. Ernzerhof, *Phys. Rev. Lett.*, 1996, **77**, 3865–3868.
47 C. Delacourt, L. Laffont, R. Bouchet, C. Wurm, J.-B. Leriche, M. Morcrette, J.-M. Tarascon and C. Masquelier, *J. Electrochem. Soc.*, 2005, **152**, A913.
48 R. A. Serway and J. W. Jewett, *Principles of Physics: A Calculus-Based Text*, Brooks/Cole, Cengage Learning, Boston, MA, 2013.
49 F. A. Kröger, *The chemistry of imperfect crystals*, North-Holland Pub. Co., American Elsevier, Amsterdam, New York, 1973.
50 O. Gerbig, R. Merkle and J. Maier, *Adv. Mater.*, 2013, **25**, 3129–3133.
51 L. Zhong, R. R. Mitchell, Y. Liu, B. M. Gallant, C. V. Thompson, J. Y. Huang, S. X. Mao and Y. Shao-Horn, *Nano Lett.*, 2013, **13**, 2209–2214.
52 G. M. Veith, J. Nanda, L. H. Delmau and N. J. Dudney, *J. Phys. Chem. Lett.*, 2012, **3**, 1242–1247.
53 B. D. Mccloskey, A. Speidel, R. Scheffler, D. C. Miller, V. Viswanathan, J. S. Hummelshøj, J. K. Nørskov and A. C. Luntz, *J. Phys. Chem. Lett.*, 2012, **3**, 997–1001.
54 B. D. McCloskey, D. S. Bethune, R. M. Shelby, T. Mori, R. Scheffler, A. Speidel, M. Sherwood and A. C. Luntz, *J. Phys. Chem. Lett.*, 2012, **3**, 3043–3047.
55 L. Nazar, B. Adams, R. Black, C. Radtke, K. Zaghib and M. Trudeau, *Energy Environ. Sci.*, 2013, **6**, 1772.
56 R. Ramprasad, H. Zhu, P. Rinke and M. Scheffler, *Phys. Rev. Lett.*, 2012, **108**, 1–5.
57 P. Mori-Sánchez, A. Cohen and W. Yang, *Phys. Rev. Lett.*, 2008, **100**, 146401.
58 M. Shishkin and G. Kresse, *Phys. Rev. B: Condens. Matter Mater. Phys.*, 2007, **75**, 1–9.
59 N. A. Deskins and M. Dupuis, *J. Phys. Chem. C*, 2008, **113**, 346–358.
60 J. Adams and M. Karulkar, *J. Power Sources*, 2012, **199**, 247–255.
61 T. Kudo and K. Fueki, *Solid State Ionics*, Kodansha VCH, Tokyo, Japan Weinheim, FRG, New York, NY, USA, 1990.
62 R. R. Mitchell, B. M. Gallant, Y. Shao-horn and C. V. Thompson, *J. Phys. Chem. Lett.*, 2013, **4**, 1060–1064.
63 A. U. Khan and S. D. Mahanti, *J. Chem. Phys.*, 1975, **63**, 2271.
64 K. Abraham and Z. Jiang, *J. Electrochem. Soc.*, 1996, **143**, 1–5.
65 T. Ogasawara, A. Débart, M. Holzapfel, P. Novák and P. G. Bruce, *J. Am. Chem. Soc.*, 2006, **128**, 1390–1393.
66 Y.-C. Lu, H. A. Gasteiger, M. C. Parent, V. Chiloyan and Y. Shao-Horn, *Electrochem. Solid-State Lett.*, 2010, **13**, A69.
67 W. Xu, K. Xu, V. V. Viswanathan, S. A. Towne, J. S. Hardy, J. Xiao, Z. Nie, D. Hu, D. Wang and J.-G. Zhang, *J. Power Sources*, 2011, **196**, 9631–9639.
68 Q. Sun, Y. Yang and Z.-W. Fu, *Electrochem. Commun.*, 2012, **16**, 22–25.
69 P. Hartmann, C. L. Bender, M. Vračar, A. K. Dürr, A. Garsuch, J. Janek and P. Adelhelm, *Nat. Mater.*, 2013, **12**, 228–32.
70 X. Ren and Y. Wu, *J. Am. Chem. Soc.*, 2013, **135**, 2923–6.
71 M. N. Obrovac, R. a. Dunlap, R. J. Sanderson and J. R. Dahn, *J. Electrochem. Soc.*, 2001, **148**, A576.
72 P. Poizot, S. Laruelle, S. Grugeon, L. Dupont and J. M. Tarascon, *Nature*, 2000, **407**, 496–499.
73 G. Cohn and Y. Ein-Eli, *J. Power Sources*, 2010, **195**, 4963–4970.
74 J. Yang, D. Zhai, H.-H. Wang, K. C. Lau, J. A. Schlueter, P. Du, D. J. Myers, Y.-K. Sun, L. A. Curtiss and K. Amine, *Phys. Chem. Chem. Phys.*, 2013, **15**, 3764–71.
75 K. C. Lau, R. S. Assary, P. Redfern, J. Greeley and L. a. Curtiss, *J. Phys. Chem. C*, 2012, **116**, 23890–23896.
76 N.-G. Vannerberg, in *Progress in Inorganic Chemistry*, John Wiley & Sons, Inc., 1962, pp. 125–197.
77 A. V. Chadwick, K. W. Flack, J. H. Strange and J. Harding, *Solid State Ionics*, 1988, **28-30**, 185–188.
78 P. W. M. Jacobst and M. L. Vernont, *J. Chem. Soc., Faraday Trans.*, 1990, **86**, 1233–1238.